



Title	Engineered dextranase from <i>Streptococcus mutans</i> enhances the production of longer isomaltooligosaccharides
Author(s)	Klahan, Patcharapa; Okuyama, Masayuki; Jinnai, Kohei; Ma, Min; Kikuchi, Asako; Kumagai, Yuya; Tagami, Takayoshi; Kimura, Atsuo
Citation	Bioscience biotechnology and biochemistry, 82(9), 1480-1487 https://doi.org/10.1080/09168451.2018.1473026
Issue Date	2018-09
Doc URL	http://hdl.handle.net/2115/74378
Rights	This is an Accepted Manuscript of an article published by Taylor & Francis in Bioscience biotechnology and biochemistry on 26/05/2018, available online: http://www.tandfonline.com/10.1080/09168451.2018.1473026 .
Type	article (author version)
File Information	FinalFile_SmDex_v7_r1_v9.pdf



[Instructions for use](#)

1 **Engineered dextranase from *Streptococcus mutans* enhances the**
2 **production of longer isomaltooligosaccharides**

3 Patcharapa Klahan, Masayuki Okuyama*, Kohei Jinnai, Min Ma, Asako
4 Kikuchi, Yuya Kumagai, Takayoshi Tagami and Atsuo Kimura*

5 *Research Faculty of Agriculture, Hokkaido University, Sapporo, Japan*

6
7 email addresses: PK, patchakl@abs.agr.hokudai.ac.jp; MO, okuyama@abs.agr.hokudai.ac.jp;
8 KJ, jin-chan@abs.agr.hokudai.ac.jp; MM, mamin@abs.agr.hokudai.ac.jp; AsakoK,
9 akikuchi@abs.agr.hokudai.ac.jp; YK, ykumagai@abs.agr.hokudai.ac.jp; TT,
10 tagami@abs.agr.hokudai.ac.jp; AtsuoK, kimura@abs.agr.hokudai.ac.jp

11
12 *Corresponding authors: Dr. Masayuki Okuyama; Kita-9 Nishi-9, Kita-ku, Sapporo
13 060-8589, Japan; Tel: +81-11-706-2816; email: okuyama@abs.agr.hokudai.ac.jp
14 Prof. Atsuo Kimura; Kita-9 Nishi-9, Kita-ku, Sapporo 060-8589, Japan; Tel/Fax: +81-
15 11-706-2808; email: kimura@abs.agr.hokudai.ac.jp

16
17 Abbreviations: CI, cycloisomaltooligosaccharide; CITase, CI glucanotransferase; CITase-Bc,
18 CITase from *Bacillus circulans* T-3040; DP, degree of polymerization of glucose unit; GH,
19 glycoside hydrolase family; GTF, glucansucrase; HPAEC-PAD, high performance anion-
20 exchange chromatography-pulsed amperometric detection; IG, isomaltooligosaccharide;
21 IG_n, IG with DP of n (n, 2–5); PNP, *p*-nitrophenol; PNP-Glc, *p*-nitrophenyl α -glucoside;
22 PNP-IG, *p*-nitrophenyl isomaltooligosaccharide; PNP-IG_n, PNP-IG with DP of n (n, 2–6);
23 SmDex, dextranase from *Streptococcus mutans*; SmDexTM, *S. mutans* ATCC25175
24 SmDex bearing Gln100–Ile732

27 **Engineered dextranase from *Streptococcus mutans* enhances the** 28 **production of longer isomaltooligosaccharides**

29 Herein, we investigated enzymatic properties and reaction specificities of
30 *Streptococcus mutans* dextranase, which hydrolyzes α -(1 \rightarrow 6)-glucosidic linkages
31 in dextran to produce isomaltooligosaccharides. Reaction specificities of wild-
32 type dextranase and its mutant derivatives were examined using dextran and a
33 series of enzymatically prepared *p*-nitrophenyl α -isomaltooligosaccharides. In
34 experiments with 4-mg \cdot mL⁻¹ dextran, isomaltooligosaccharides with degrees of
35 polymerization (DP) of 3 and 4 were present at the beginning of the reaction, and
36 glucose and isomaltose were produced by the end of the reaction. Increased
37 concentrations of the substrate dextran (40 mg \cdot mL⁻¹) yielded
38 isomaltooligosaccharides with higher DP, and the mutations T558H,
39 W279A/T563N, and W279F/T563N at the -3 and -4 subsites affected hydrolytic
40 activities of the enzyme, likely reflecting decreases in substrate affinity at the -4
41 subsite. In particular, T558H increased the proportion of isomaltooligosaccharide
42 with DP of 5 in hydrolysates following reactions with 4-mg \cdot mL⁻¹ dextran.

43 **Key words:** glycoside hydrolase family 66; dextranase;
44 isomaltooligosaccharides; bond cleavage frequency

45 **Introduction**

46 Dextranase (6- α -D-glucan 6-glucanohydrolase, EC 3.2.1.11) catalyzes the
47 endohydrolysis of α -(1 \rightarrow 6)-glucosidic linkages in dextran. According to classifications
48 of the glycoside hydrolase family (GH), GH49, GH31, and GH66 groups include
49 dextranases [1]. The GH49 is a group of an inverting dextranases, whereas exo-type α -
50 glucosidases predominate in the GH31 group and the recently discovered endo-type
51 dextranase [2] is a unique member in this family. The GH66 group includes the dextran-
52 active enzymes dextranase and cycloisomaltooligosaccharide glucanotransferase
53 (CITase; (1 \rightarrow 6)- α -D-glucan:(1 \rightarrow 6)- α -D-glucan 6- α -D-[1 \rightarrow 6 α -D-glucano]-transferase
54 (cyclizing), EC 2.4.1.248), which converts dextran to cycloisomaltooligosaccharides

55 (CIs) using an intramolecular transglycosylation mechanism [3]. CITase was originally
56 identified in *Bacillus* spp (currently *Bacillus circulans* T-3040), and the enzyme
57 catalyzes the formation of cycloisomalto-heptaose (CI-7), -octaose (CI-8), and -nonaose
58 (CI-9) [4]. Several crystal structures of GH66 enzymes have been determined
59 previously [5–8], and $(\beta/\alpha)_8$ barrel-fold domains were identified as catalytically relevant.
60 The characteristic architecture of CITase includes a β -jellyroll-fold domain (domain B),
61 which is inserted at the $\beta \rightarrow \alpha$ loop 7 of the catalytic domain [6,8]. This domain B was
62 categorized as a member of the carbohydrate-binding module family 35, and was shown
63 to recruit substrates and maintain product sizes during the formation of CIs [9].
64 However, this domain was not found in dextranase structures [5,7].

65 *Streptococcus mutans* (*S. mutans*) expresses glucansucrases (GTFs) that
66 synthesize high molecular weight sticky glucans from sucrose, and these contribute to
67 adherence of bacteria in dental caries [10,11]. Among GTFs, GTF-I, and GTF-SI are
68 predominantly associated with the formation of insoluble glucan with α -(1 \rightarrow 3)-
69 glucosidic linkages, whereas GTF-S contributes to the synthesis of dextran, which is a
70 water-soluble glucan [10]. *S. mutans* also expresses dextran degrading enzymes, an
71 extracellular dextranase (SmDex), and an intracellular glucan α -1,6-glucosidase [12].
72 SmDex produces isomaltooligosaccharides (IGs) from dextran, and these are ingested
73 by bacteria and then degraded to glucose by glucan α -1,6-glucosidase.

74 IGs have reported prebiotic effects [13,14], and oligosaccharides with α -(1 \rightarrow 6)-
75 glucosidic linkages are generally synthesized by α -glucosidase-catalyzed
76 transglucosylation from maltooligosaccharides. However, following these reactions,
77 some IGs include the α -(1 \rightarrow 4)-glucosidic linkage [15], thus limiting the purity of the
78 resulting IGs. In contrast, dextranase only produces IGs with α -1,6-glucosidic linkages.
79 In recent years, commercial grade IGs products have become indispensable for research

80 in fields such as biochemistry and food science, but remain difficult to obtain. Thus, we
81 refined the methods for producing IGs of various sizes by improving the function of
82 SmDex with site-specific mutations. Prior to these manipulations, three-dimensional
83 structures of GH66 [5,6] were used to predict amino acid residues that are responsible
84 for product specificity.

85 As reported previously [16], we produced recombinant full-size SmDex protein
86 in *Escherichia coli* and showed that it is subject to proteolysis, whereas N- and C-
87 terminal truncated SmDex (SmDexTM; bearing Gln100–Ile732) proteins are not. Thus,
88 SmDexTM was used as the parent enzyme, and patterns of hydrolytic activities were
89 compared with those of SmDexTM derivatives by analyzing reactions with synthesized
90 *p*-nitrophenyl isomaltooligosaccharides (PNP-IGs) and by examining carbohydrate
91 compositions of the resulting dextran hydrolysates.

92 **Materials and methods**

93 *Production of SmDexTM and its mutant derivatives*

94 A pET28a-derived plasmid containing the SmDexTM coding sequence [16] was used as
95 the template for site-directed mutagenesis, which was performed according to the
96 PrimeSTAR Mutagenesis Basal Kit manual (Takara Bio, Shiga, Japan). Site directed
97 mutagenesis was performed using the following oligonucleotides:

98 5'-GTTTGATGACCTGTTCAATCGGCAGGTTGAAACAGATGC-3' and 5'-

99 CAACCTGCCGATTGAACAGGTCATCAAACCTTAGGAAC-3' for MT-1; 5'-

100 TTGATGACCTGAGCCATTCGCAGGTTGAAAC-3' and 5'-

101 GGCTCAGGTCATCAAACCTTAGGAACATTAG-3' for MT-2; 5'-

102 ACCTGTTCAATTCGCAGGTTGAAACAGATGC-3' and 5'-

103 GCGAATTGAACAGGTCATCAAACCTTAGG-3' for MT-3; 5'-

104 TCAATCGGCAGGTTGAAACAGATGCTG-3' and 5'-
105 CAACCTGCCGATTGAACAGGTCATCAAAC for MT-4; 5'-
106 TGGAATGCGTGGAGCCATTCGCAG-3' and 5'-
107 GCTCCACGCATTCCAAGACTGATCAAA-3' for W279A; 5'-
108 TGGAATTTGTGGAGCCATTCGCAG-3' and 5'-
109 GCTCCACAAATTCCAAGACTGATCAAA-3' for W279F; 5'-
110 CTTAGAACACGCTTATTATCCAACACAA-3' and 5'-
111 AATAAGCGTGTTCTAAGACACCGACACC-3' for T558H; and 5'-
112 TATCCAAACCAAAGCCTCAAGGTTTCG-3' and 5'-
113 GCTTTGGTTTGGATAATAAGCTGTTTC-3' for T563N. Mutations were then
114 confirmed at the DNA Sequencing Facility of the Research Faculty of Agriculture,
115 Hokkaido University (ABI 3100 Genetic Analyzer; Applied Biosystems/Thermo,
116 Carlsbad, CA, USA). Enzymes were produced and purified as described in our previous
117 report [16].

118 *Enzyme assays*

119 Enzyme activity was measured at 35°C for 8 min using a standard reaction mixture
120 comprising 4-mg·mL⁻¹ dextran (MW of 15,000–20,000 was used throughout; Nacalai
121 Tesque, Kyoto, Japan), 40 mM sodium acetate buffer (pH 5.0), and enzymes at
122 appropriate concentrations. Reactions were terminated by incubating at 100°C for 10
123 min and reducing sugars were determined using the copper-bicinchoninate method with
124 glucose as the standard carbohydrate. One unit of enzyme activity was defined as the
125 amount of enzyme that produces 1 μmol of reducing sugar per min under standard
126 conditions.

127 The effects of pH on rates of dextran hydrolysis were examined under standard
128 assay conditions with the Britton-Robinson buffer at pH 2.0–10.0. The buffer contained
129 40 mM acetic acid, 40 mM phosphoric acid, and 40 mM boric acid, and the pH was
130 adjusted using 0.2 M NaOH. For measurements of pH stability, SmDexTM (88 nM),
131 W279A (91 nM), W279F (78 nM), T563N (72 nM), W279F/T563N (30 nM),
132 W279A/T563N (46 nM), or T558H (50 nM) were incubated in Britton-Robinson buffer
133 at 4°C for 24 h, followed by measurements of residual activity under standard assay
134 conditions. The stable region was defined as the pH range with residual activity of >
135 90%. To determine thermal stability, SmDexTM (88 nM), W279A (91 nM), W279F (78
136 nM), T563N (72 nM), W279F/T563N (30 nM), W279A/T563N (46 nM), and T558H
137 (50 nM) were stored in 40 mM sodium acetate buffer (pH 5.0) at 15, 20, 30, 40, 50, and
138 60°C for 15 min, and residual activities were then measured under standard conditions.
139 Stable temperature regions were defined as those in which residual activity was > 90%.

140 The kinetic parameters k_{cat} and K_m were calculated using KaleidaGraph 3.6 J
141 (Synergy Software, Reading, PA, USA) from a weighted Michaelis-Menten fit of initial
142 velocities at dextran concentrations of 1.0–8.0 mg·mL⁻¹ (SmDexTM), 2.0–14 mg·mL⁻¹
143 (W279F), 2.0–12 mg·mL⁻¹ (W279A), 1.0–14 mg·mL⁻¹ (T563N), 1.0–35 mg·mL⁻¹
144 (W279F/T563N), 1.0–40 mg·mL⁻¹ (W279A/T563N), and 1.0–14 mg·mL⁻¹ (T558H).
145 All experiments were repeated three times and data are presented as means and standard
146 deviations. k_{cat}/K_m values were estimated from mean values of k_{cat} and K_m , and enzyme
147 concentrations in reaction mixtures were 88 (SmDexTM), 91 (W279A), 78 (W279F),
148 72 (T563N), 30 (W279F/T563N), 46 (W279A/T563N), and 50 nM (T558H).

149 ***Bond cleavage frequency analyses***

150 To determine bond cleavage frequencies, we measured initial hydrolysis velocities of *p*-

151 nitrophenyl α -isomalto-trioside (PNP-IG3), -tetraoside (PNP-IG4), -pentaoside (PNP-
152 IG5), and -hexaoside (PNP-IG6). Reaction mixtures contained substrates at 1 mM,
153 enzymes (SmDexTM, 18, 2.5, 1.3, and 0.30 μ M; W279A, 18, 9.0, 2.6, and 0.29 μ M;
154 W279F, 16, 7.8, 2.0, and 0.39 μ M; T558H, 10, 5.0, 1.4, and 0.42 μ M; T563N, 14, 7.2,
155 1.8, and 0.29 μ M; W279A/T563N, 9.3, 4.6, 1.3 and, 0.23 μ M; W279F/T563N, 5.9, 3.0,
156 0.74, and 0.20 μ M for PNP-IG3, -IG4, -IG5, and -IG6, respectively), and 40 mM
157 sodium acetate buffer (pH 5.0), and were incubated at 35°C. After 2 and 20 min,
158 reactions were terminated by incubating at 100°C for 10 min. The reaction products
159 were the analyzed using a Jasco HPLC system (Jasco, Tokyo, Japan) equipped with a
160 Unison UK-C18 column (ID 4.6 \times 250 mm; Imtakt, Kyoto, Japan), and with an isocratic
161 mobile phase comprising 9:91 (v/v) acetonitrile:water at a flow rate of 0.5 mL \cdot min⁻¹ at
162 50°C. Subsequently, *p*-nitrophenyl α -glucoside (PNP-Glc) and PNP-IGs (PNP-IG2–
163 PNP-IG5) were detected at 313 nm, and their concentrations were determined from
164 peak areas using BORWIN/HSS-2000 software (Jasco). Quantitative *p*-nitrophenol
165 (PNP) release was estimated according to absorption at 400 nm in the presence of 667
166 mM sodium carbonate. PNP-IG2 was prepared as described previously [17,18]. PNP-
167 IG3, -IG4, -IG5, and -IG6 were synthesized from PNP-Glc (12 mM, Nacalai Tesque) by
168 transglucosylation of laboratory-owned oligo-1,6-glucosidase (43 nM). Products were
169 then separated by gel filtration column chromatography using a BioGel P2 column (ID
170 16 \times 1,870 mm; Bio-Rad, Hercules, CA, USA) and ESI-MS spectra of purified PNP-
171 IG3–PNP-IG6 were recorded using an Exactive instrument (Thermo Fisher Scientific,
172 Waltham, MA, USA). PNP-IG3, *m/z* calculated: 624.19 [M–H]⁻, found: 624.18; PNP-
173 IG4, *m/z* calculated: 786.24 [M–H]⁻, found: 786.23; PNP-IG5, *m/z* calculated: 948.29
174 [M–H]⁻, found: 948.29; PNP-IG6, *m/z* calculated: 1,110.34 [M–H]⁻, found: 1,110.34.
175 Prior to determining hydrolytic products, isomaltohexose was prepared by partial acid

176 hydrolysis of dextran and was separated by gel filtration column chromatography using
177 a BioGel P2 column.

178 *Analysis of Dextran hydrolysates*

179 Enzymes (780 nM) were incubated with 4-or 40-mg·mL⁻¹ dextran in 40 mM sodium
180 acetate buffer (pH 5.0) at 35°C. Reactions were terminated by incubating at 100°C for
181 10 min, and products were quantified using high performance anion-exchange
182 chromatography-pulsed amperometric detection (HPAEC-PAD; Dionex ICS-3000
183 system; Dionex/Thermo, Idstein, Germany) with a CarboPac PA-1 column (ID 4 × 250
184 mm; Dionex/Thermo). Carbohydrates were separated by isocratic elution with 400 mM
185 sodium hydroxide at a flow rate of 0.8 mL·min⁻¹.

186 **Results and discussion**

187 *Selection of target residues for modifications of reaction specificity*

188 The -3 and -4 subsites of SmDex were selected to transform subsite affinities and alter
189 reaction specificities. Such transformations should yield dextran hydrolysates with
190 differing degrees of polymerization of glucose units (DP) than that achieved using
191 native SmDex. SmDexTM has Trp279, Trp280, Thr558, Tyr560, and Thr563 residues
192 in the vicinity of the -3 and -4 subsites [5] (Fig. 1A). Trp279 and Trp280 are located at
193 the β→α loop 2 of the catalytic (β/α)₈ barreled domain, whereas the other three amino
194 acids are located at the β→α loop 8. The crystal structure of CITase was used as a
195 reference to select residues to mutate. CITase catalyzes the formation of CI-7, -8, and -9,
196 suggesting the presence of minus subsites that can accommodate isomaltooligosyl
197 residues with high DP. In *Bacillus circulans* T-3040 CITase (CITase-Bc), Phe207,
198 His579, Tyr581, and Asn584 are associated with the formation of -3 and -4 subsites [6]

199 (Fig. 1A). Because His579 and Asn584 are part of the $\beta \rightarrow \alpha$ loop 8 and correspond with
200 Thr558 and Thr563 of SmDexTM, we generated corresponding T558H and T563N
201 mutations. The architecture of the $\beta \rightarrow \alpha$ loop 2 of CITase-Bc is distinct from the
202 corresponding loop of SmDexTM, and is four residues longer in SmDexTM (Fig. 1A,
203 B). Thus, the SmDexTM mutants MT-1, MT-2, MT-3, and MT-4 were generated with
204 the CITase-like structure (Fig. 1B). MT-1 with a $\beta \rightarrow \alpha$ loop 2 of the same length as
205 CITase-Bc was generated to analyze the effects of loop lengths on specificity, and MT-
206 2, MT-3, and MT-4 were then prepared by imposing point mutations on MT-1.
207 However, hydrolytic activities of these proteins were below the detection limit and
208 kinetic analyses of the contribution of the $\beta \rightarrow \alpha$ loop 2 on specificity were not possible.
209 Thus, we constructed W279A and W279F to assess the effects of the $\beta \rightarrow \alpha$ loop 2 on
210 specificity. Of the two tryptophans located within the $\beta \rightarrow \alpha$ loop 2, Trp279 is unique in
211 SmDex and in related species (Fig. 1B), and was chosen as the target residue for
212 analyses of the influence of loop 2 divergences. In addition, the double mutants
213 W279F/T563N and W279A/T563N were designed to investigate the effects of
214 mutations at both the $\beta \rightarrow \alpha$ loop 2 and $\beta \rightarrow \alpha$ loop 8. CITase-Bc carries Phe501, Asp512,
215 and Trp514 in domain B, and these residues are parts of subsites -3 and -4 (Fig. 1A).
216 However, these residues were excluded from our mutation analyses because SmDexTM
217 does not have the corresponding domain.

218 ***Production of recombinant enzymes and their characterization***

219 The aforementioned 10 mutants were produced in *E. coli* with SmDexTM [16] as the
220 parent enzyme. As mentioned above, hydrolytic activities of MT-1, MT-2, MT-3, and
221 MT-4 proteins were undetectable, and specific activities of W279A and W279F were
222 almost similar to that of SmDexTM. The specific activity of T563N was 50% less than

223 that of the parent enzyme, and other variants showed activity decreases between 8% and
224 20% (Table 1). No mutant enzymes produced detectable amounts of CI. The optimal pH
225 for SmDexTM and its derivatives was 5.0, whereas that for T558H was 4.2. These
226 mutations showed minimal influences on pH stability ranges when compared with that
227 of the parent enzyme, and thermal stabilities of the mutants were almost identical to that
228 of SmDexTM (Table 1).

229 Table 2 summarizes the kinetic parameters for hydrolysis of dextran by
230 SmDexTM and the present mutants. Hydrolytic rates in the presence of various dextran
231 concentrations followed Michaelis-Menten relationships, and K_m values were greater for
232 all mutants than for SmDexTM, and remarkable increases were observed for the double
233 mutants W279A/T563N and W279F/T563N. Double replacements at Trp279 and
234 Thr563 affected the formation of the ES complex, although k_{cat} values of most of these
235 mutants varied between 65% and 145% of parent protein values. Only the mutant
236 T558H gave a much lower value (41%) when compared with the parent protein, and the
237 mutation to Thr558 likely affected the reactivity of the ES complex and/or the product
238 release step from the EP complex.

239 Hydrolytic products of SmDexTM with 1 mM isomaltohexaose (IG6) were
240 monitored using HPAEC-PAD, and productions of glucose, isomaltose (IG2), isomalto-
241 triose (IG3) -tetraose (IG4), and -pentaose (IG5) were observed. Production rates of
242 glucose, IG2, and IG3 were 1.61 ± 0.15 , 1.52 ± 0.05 , and 0.548 ± 0.041 $\mu\text{mol}/\text{min}/\text{mg}$
243 protein, respectively. Because two moles of IG3 are produced from one mole of IG6,
244 the calculated intrinsic rate of IG3 production is 0.274 $\mu\text{mol}/\text{min}/\text{mg}$. Except for the
245 reaction that generate IG3, IG6 has two binding modes and these were indistinguishable
246 in these experiments (Fig. 2A). Accordingly, our analyses give limited information
247 about hydrolytic patterns of SmDexTM in the presence of IG6. Further experiments

248 using [¹⁴C]glucose labeled IGs may reveal their binding modes, as shown in a reported
249 [19] analysis of action patterns and subsite maps of *S. mutans* KI-R dextranase.

250 ***Analysis of bond cleavage frequencies by SmDexTM and its mutants using***
251 ***PNP-IGs***

252 In this study, we developed a method for estimating binding modes of substrate to
253 SmDexTM using a series of PNP-IGs instead of radioactive substrate. PNP-IGs readily
254 enabled the identification of cleavage sites and quantification of their hydrolytic
255 products with the chromogenic PNP group using a RP-HPLC–UV detector. Thus, a
256 series of PNP-IGs were enzymatically prepared and initial rates of SmDexTM mediated
257 hydrolysis of 1 mM PNP-IG3–PNP-IG6 were determined (Fig. 2B). The enzyme
258 hydrolyzed all PNP-IGs except PNP-IG3, and the highest hydrolytic rate of SmDexTM
259 was achieved with PNP-IG6. In addition, the enzyme produced only PNP-Glc from
260 PNP-IG4, and preferentially released PNP-Glc with small amounts of PNP-IG3 from
261 PNP-IG5 or PNP-IG6. SmDexTM did not yield detectable amounts of PNP or PNP-IG2
262 in catalysis of any of the present PNP-IGs substrates.

263 Binding of PNP to subsites may influence functional evaluations of PNP-IGs in
264 analyses of hydrolytic patterns of SmDexTM, because PNP is a mimic of glucosyl
265 moieties. The failure of PNP production from PNP-IG5, however, disagrees with
266 production of glucose from IG6 (Fig. 2A), indicating that SmDexTM cannot hydrolyze
267 the heteroside linkage between α -glucoside and PNP. In contrast, other enzymes with
268 specificity toward α -(1→6)-glucosidic linkages, such as glucan α -1,6-glucosidase and
269 oligo-1,6-glucosidase, can hydrolyze these heteroside linkages [17, 20]. However,
270 SmDex likely has a more rigid +1 subsite than those of α -(1→6)-specific enzymes, and
271 hence, exhibits strict specificity toward the α -(1→6)-glucosidic linkage. Moreover, the
272 lack of PNP-IG2 production from PNP-IG5 reflects lower production of IG3, rather

273 than low production of glucose and IG2 from IG6 (Fig. 2A). Additionally, the +3
274 subsite may not be suitable for PNP, because PNP-IG2 was not produced from any
275 other PNP-IGs. Three-dimensional structures of SmDex with bound ligands to plus
276 subsites are not available and the details of substrate binding to plus subsites remain
277 unknown. However, Trp455 and Phe457 are expected to be located at plus subsites [5],
278 and interactions, such as π - π interactions, of their side chains with PNP may facilitate
279 binding of PNP to plus subsites other than the +3 subsite.

280 As with SmDexTM, all mutant enzymes exhibited higher hydrolytic rates
281 toward PNP-IG6 than toward PNP-IG5 and PNP-IG4, and no activity toward PNP-IG3
282 (Fig. 3). The hydrolytic pattern of W279A was similar to that of SmDexTM, whereas
283 those of W279F, T563N, W279F/T563N, W279A/T563N, and T558H were altered (Fig.
284 3). In these variants, proportions of released PNP-Glc were decreased following
285 hydrolysis of PNP-IG5 and PNP-IG6. In particular, significant decreases in the
286 proportion of PNP-Glc was noted in W279F/T563N, W279A/T563N, and T558H when
287 PNP-IG6 was used as the substrate (Fig. 3). In these three mutants, percentage
288 velocities of PNP-Glc were less than that of PNP-IG3, and it is assumed that these
289 mutations decreased the affinity at the -4 subsite, leading to changes in the binding
290 mode of PNP-IG6. Alternatively, we suggest that reduced affinity at the -5 subsite may
291 also change the hydrolytic action patterns. However, during hydrolysis of PNP-IG5,
292 decreased affinity at the -5 subsite is unlikely to increase the proportion of released
293 PNP-IG3, suggesting that the decrease in -4 subsite affinity reflects changes in the
294 binding modes of PNP-IG5 and PNP-IG6.

295 Mutation related changes in hydrolysis rates with the present PNP-IGs were
296 smaller than those with dextran (Table 1), suggesting that the decreases in observed
297 hydrolytic rates are related to the size of the substrate. During hydrolysis of dextran, all

298 subsites are occupied by the substrate, and mutations of subsites measurably influenced
299 the hydrolysis of dextran. In contrast, subsite-binding modes of PNP-IGs can be
300 changed by selecting a high affinity-binding mode, which only leads to small decreases
301 in reaction rates of mutants. To evaluate the effects of changes in subsite affinities, we
302 should determine kinetic parameters for hydrolysis of PNP-IGs as well as dextran.
303 However, it was difficult to determine K_m values for the series of PNP-IGs, because rate
304 estimates were hampered by multiple degradation modes.

305 Herein, we formed PNP conjugates to facilitate detection of hydrolytic products,
306 but found that these influenced PNP-IG binding to plus subsites. However, reductions in
307 affinities of PNP-IGs for mutant minus subsites could be detected, indicating that PNP-
308 IGs are suitable for assessments of minus subsites of dextranases, including SmDex.

309 *Analysis of dextran hydrolysates in reactions of SmDexTM and its mutants*

310 Dextran (4 or 40 mg·mL⁻¹) was hydrolyzed by SmDexTM, and the resulting
311 carbohydrate compositions in 2, 8, and 24-h reaction mixtures were analyzed using
312 HPAEC-PAD. With an initial dextran concentration of 4 mg·mL⁻¹, the 2-h reaction
313 mixture with SmDexTM predominantly contained IG2, IG3, and IG4, with trace
314 concentrations of IG5 (Fig. 4A). Following longer reaction times, percentage of glucose
315 and IG2 contents of reaction mixtures increased, whereas those of IG3 and IG4
316 decreased. In the 24-h reaction mixture, 83% of the dextran had been converted,
317 predominantly to glucose and IG2, and increases in mono- and disaccharide
318 concentrations followed further hydrolysis of the intermediates IG3, IG4, and IG5.
319 Bond cleavage frequency analyses demonstrated that SmDexTM failed to hydrolyze
320 PNP-IG3, but hydrolyzed IG3 into glucose and IG2. In subsequent experiments,
321 increased initial dextran concentrations of 40 mg·mL⁻¹ led to lower concentration ratios

322 of glucose and increased ratios of IG5, which was degraded with longer reaction times
323 (Fig. 4B). In these reactions, 83% of dextran was consumed after 24 h incubation and
324 ratios of IG3 and IG4 were higher than in reactions containing 4 mg·mL⁻¹ dextran.
325 Therefore, high dextran concentrations are suitable for obtaining IGs with high DP
326 using SmDexTM.

327 To examine dextran hydrolysis by the present mutants, we determined
328 hydrolysate concentrations after reactions. The effects of the present mutations were
329 prominent at a dextran concentration of 4 mg·mL⁻¹ (Fig. 4A), and ratios of IGs were
330 higher following reactions with mutants than with SmDexTM. In W274A/F, almost half
331 of the products were IG2 and IG3 in 24-h reactions, and about 80% of the dextran was
332 degraded. In contrast, negligible amounts of IG3 remained following reactions with the
333 parent enzyme, and 24-h reaction mixtures of W274F/T563N and W274A/T563N had
334 carbohydrate compositions similar to those of W274A/F, whereas that of T563N was
335 similar to hydrolysates from SmDexTM reactions. These data indicate that the Trp279
336 mutation strongly influences the characteristics of double mutant enzymes. T558H
337 showed a carbohydrate composition that was distinctly different from the parent enzyme.
338 Specifically, almost 50% of the dextran in the reaction mixture was degraded after 2 h,
339 and high proportions of IGs were observed, predominantly IG5. In addition, IG4 remain
340 in the reaction mixture at 24 h, suggesting that decreased affinity at the -4 subsite due
341 to the substitution of His for Thr588 reduces the enzyme-substrate binding energy
342 during the hydrolysis of IG4 and IG5, and leads to reduced hydrolytic activities and
343 decreased IG consumption ratios. At a substrate concentration of 40 mg·mL⁻¹,
344 carbohydrate profiles following reactions of mutant enzymes differed little from that of
345 SmDexTM (Fig. 4B). In all cases, glucose and IG2–IG5 were detected during the early
346 stages of the reaction, and IGs with high DP decreased over time. Following 24-h

347 reactions of T563N, T558H, W279A/T563N, and W279F/T563H, ratios of IGs contents
348 were slightly higher and glucose concentrations were lower than those of the parent
349 enzyme.

350 Pronounced effects of mutations on hydrolysates at the lower concentration of
351 dextran ($4 \text{ mg}\cdot\text{mL}^{-1}$) likely correspond with differences in IGs concentrations in the
352 reaction mixture. Ratios of IGs to dextran concentrations increased more rapidly at the
353 lower dextran concentration than at the higher dextran concentration ($40 \text{ mg}\cdot\text{mL}^{-1}$). At
354 the high dextran concentration, enzyme reactions with IGs substrates are much less
355 likely, because dextran, which is the preferred substrate, remained in the reaction
356 solutions for longer period. As seen in hydrolysis experiments with PNP-IGs (Fig. 3),
357 the mutations can influence hydrolytic patterns toward IGs. Consequently, the effects of
358 mutations were more marked at the lower dextran concentration.

359 In summary, we generated several mutant enzymes according to structural
360 comparisons with CITase and evaluated their hydrolytic activities toward PNP-IGs and
361 dextran. These experiments showed that the binding mode of PNP-IG5 and -IG6
362 changed in W279F/T563N, W279A/T563N, and T558H mutant enzymes, due to
363 decreased affinities at the -4 subsite. We also showed that all variants, except for
364 T563N, generated IGs with higher DP than SmDexTM in the presence of low
365 concentrations of dextran. Finally, T558H achieved a high proportion of IG5 in reaction
366 mixtures (Fig. 4), and is therefore a promising candidate for the production of IGs with
367 high DP from dextran.

368

369 **Author contributions**

370 K.P. conducted most of the experiments and analyzed the results with help from M.O., T.T. and
371 Atsuo K. M.M., Y.K., and Asako K. were involved in analytical HPLC and HPAEC-PAD
372 analyses. K.J. contributed to the preparation of IG6. M.O. and Atsuo K. conceived the project

373 and wrote the paper with K.P. All authors have reviewed the results and approved the final
374 version of the manuscript.

375

376 **Disclosure statement**

377 No potential conflict of interest was reported by the authors.

378

379 **Acknowledgements**

380 We thank the staff of the Instrumental Analysis Division of the Creative Research Institution at
381 Hokkaido University for amino acid and mass spectrometric analyses. The authors would like to
382 thank Enago (www.enago.jp) for the English language review.

383

384 **References**

- 385 [1] Lombard V, Golaconda Ramulu H, Drula E, et al. The carbohydrate-active
386 enzymes database (CAZy) in 2013. *Nucleic Acids Res.* 2014;42:D490–D495.
- 387 [2] Gozu Y, Ishizaki Y, Hosoyama Y, et al. A glycoside hydrolase family 31
388 dextranase with high transglucosylation activity from *Flavobacterium johnsoniae*.
389 *Biosci. Biotechnol. Biochem.* 2016;80:1562–1567.
- 390 [3] Oguma T, Tobe K, Kobayashi M. Purification and properties of a novel enzyme
391 from *Bacillus* spp. T-3040, which catalyzes the conversion of dextran to cyclic
392 isomaltooligosaccharides. *FEBS Lett.* 1994;345:135–138.
- 393 [4] Oguma T, Horiuchi T, Kobayashi M. Novel Cyclic Dextrins,
394 Cycloisomaltooligosaccharides, from *Bacillus* sp. T-3040 Culture. *Biosci.*
395 *Biotechnol. Biochem.* 1993;57:1225–1227.
- 396 [5] Suzuki N, Kim YM, Fujimoto Z, et al. Structural elucidation of dextran
397 degradation mechanism by *Streptococcus mutans* dextranase belonging to
398 glycoside hydrolase family 66. *J. Biol. Chem.* 2012;287:19916–19926.
- 399 [6] Suzuki N, Fujimoto Z, Kim YM, et al. Structural elucidation of the cyclization
400 mechanism of α -1,6-glucan by *Bacillus circulans* T-3040
401 cycloisomaltooligosaccharide glucanotransferase. *J. Biol. Chem.*
402 2014;289:12040–12051.

- 403 [7] Suzuki N, Kishine N, Fujimoto Z, et al. Crystal structure of thermophilic
404 dextranase from *Thermoanaerobacter pseudethanolicus*. *J. Biochem.*
405 2015;159:331–339.
- 406 [8] Fujimoto Z, Kishine N, Suzuki N, et al. Isomaltooligosaccharide-binding
407 structure of *Paenibacillus* sp. 598K cycloisomaltooligosaccharide
408 glucanotransferase. *Biosci. Rep.* 2017;37:BSR20170253.
- 409 [9] Suzuki R, Suzuki N, Fujimoto Z, et al. Molecular engineering of
410 cycloisomaltooligosaccharide glucanotransferase from *Bacillus circulans* T-3040:
411 structural determinants for the reaction product size and reactivity. *Biochem. J.*
412 2015;467:259–270.
- 413 [10] Monchois V, Willemot RM, Monsan P. Glucansucrases: mechanism of action
414 and structure–function relationships. *FEMS Microbiol. Rev.* 1999;23:131–151.
- 415 [11] Tamesada M, Kawabata S, Fujiwara T, et al. Synergistic effects of Streptococcal
416 glucosyltransferases on adhesive biofilm formation. *J. Dent. Res.* 2004;83:874–
417 879.
- 418 [12] Colby SM, Whiting GC, Tao L, et al. Insertional inactivation of the
419 *Streptococcus mutans* dexA (dextranase) gene results in altered adherence and
420 dextran catabolism. *Microbiology (Reading, Engl.)* 1995;141:2929–2936.
- 421 [13] Kohmoto T, Fukui F, Takaku H, et al. Effect of isomalto-oligosaccharides on
422 human fecal flora. *Bifidobacteria and microflora.* 1988;7:61–69.
- 423 [14] Kohmoto T, Fukui F, Takaku H, et al. Dose-response test of
424 isomaltooligosaccharides for increasing fecal bifidobacteria. *Agric. Biol. Chem.*
425 1991;55:2157–2159.
- 426 [15] Ma M, Okuyama M, Sato M, et al. Effects of mutation of Asn694 in *Aspergillus*
427 *niger* α -glucosidase on hydrolysis and transglucosylation. *Appl. Microbiol.*
428 *Biotechnol.* 2017;101:6399–6408.
- 429 [16] Kim YM, Shimizu R, Nakai H, et al. Truncation of N- and C-terminal regions of
430 *Streptococcus mutans* dextranase enhances catalytic activity. *Appl. Microbiol.*
431 *Biotechnol.* 2011;91:329–339.

- 432 [17] Saburi W, Mori H, Saito S, et al. Structural elements in dextran glucosidase
433 responsible for high specificity to long chain substrate. *Biochim. Biophys. Acta*
434 2006;1764:688–698.
- 435 [18] Kobayashi M, Saburi W, Nakatsuka D, et al. Structural insights into the catalytic
436 reaction that is involved in the reorientation of Trp238 at the substrate-binding
437 site in GH13 dextran glucosidase. *FEBS Lett.* 2015;589:484–489.
- 438 [19] Pulkownik A, Thoma JA, Walker GJ. The action pattern and subsite map of
439 *Streptococcus mutans* K1-R dextranase. *Carbohydr. Res.* 1978;61:493–497.
- 440 [20] Okuyama M, Saburi W, Mori H, et al. α -Glucosidases and α -1,4-glucan lyases:
441 structures, functions, and physiological actions. *Cell Mol Life Sci.*
442 2016;73:2727–2751.
- 443 [21] Davies G, Wilson K, Henrissat B. Nomenclature for sugar-binding subsites in
444 glycosyl hydrolases. *Biochem. J.* 1997;321:557–559.
445

446 Table 1. Basic properties of SmDexTM and its mutant derivatives

Enzyme	Specific activity (U/mg)	Optimum pH	pH stability ^a	Thermal stability (°C) ^a
SmDex TM	58	5.0	4.0 – 9.0	< 40
W279A	43	5.0	4.0 – 10.0	< 40
W279F	46	5.0	3.0 – 10.0	< 40
T558H	11	4.2	3.5 – 8.0	< 40
T563N	27	5.0	4.0 – 9.0	< 40
W279A/T563N	6.1	5.0	4.0 – 8.0	< 40
W279F/T563N	4.7	5.0	4.0 – 8.0	< 38

447 ^a Range at which residual activity is more than 90%

448 Table 2. Kinetic parameters of SmDexTM and its mutant derivatives for the hydrolysis
 449 of dextran

Enzyme	K_m (mg·mL ⁻¹)	k_{cat} (s ⁻¹)	$\frac{k_{cat}}{K_m}$ (s ⁻¹ ·mL·mg ⁻¹)
SmDex TM	1.8 ± 0.1	77 ± 1	43
W279A	6.1 ± 0.1	99 ± 1	16
W279F	5.4 ± 0.1	110 ± 0	20
T558H	4.2 ± 0.1	29 ± 1	6.9
T563N	5.2 ± 0.5	57 ± 1	11
W279A/T563N	61 ± 1	98 ± 1	1.6
W279F/T563N	32 ± 1	50 ± 1	1.6

450 k_{cat} and K_m values are presented as means ± standard deviation of triplicate
 451 measurements.

452 **Figure captions**

453 Fig. 1. Three-dimensional structure comparisons of SmDexTM (PDB ID: 3VMN;
454 *green*) and CITase-Bc (PDB ID: 3WNL; *yellow*; A) and multiple sequence alignment of
455 a part of the $\beta \rightarrow \alpha$ loop 2 of the catalytic $(\beta/\alpha)_8$ barrel of GH66 enzymes (B)

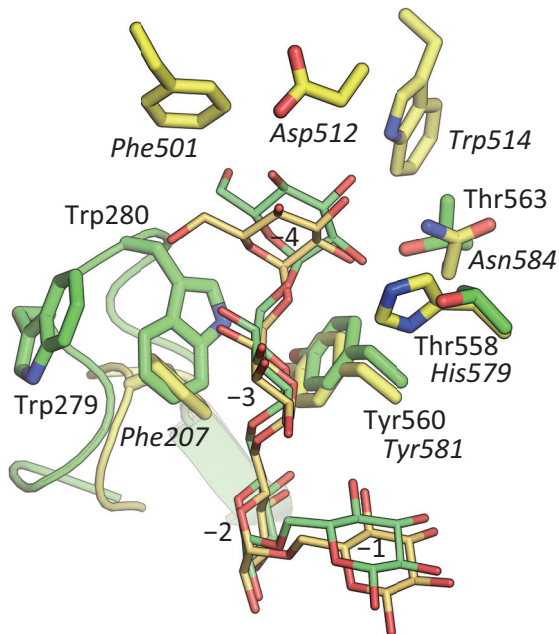
456 (A) Depicted residues are associated with the formation of -3 and -4 subsites.
457 Numbers in italics represent residues of CITase-Bc. (B) Characters on the left side
458 indicate UniProtKB accession numbers or enzymes (SmDex, MT-1–MT-4, and CITase-
459 BC). Multiple sequence alignments were performed using MAFFTash
460 (<https://sysimm.ifrec.osaka-u.ac.jp/MAFFTash/>).

461 Fig. 2. Schematics of IG6, PNP-IG4, -IG5, and -IG6 binding subsites in SmDexTM
462 Circles are glucose residues and lines between two circles show α -(1 \rightarrow 6)-glucosidic
463 linkages. The subsite number notation is in accordance with the system using “ $-n$ ” and
464 “ $+n$ ” [21]. (A) The values on the right indicate release rates of glucose (binding modes
465 1 and 2), IG2 (binding modes 3 and 4), and IG3 (binding mode 5). (B) The values on
466 the right side represent release rates of either PNP-Glc or PNP-IG3. Numbers in
467 parentheses are bond cleavage frequencies.

468 Fig. 3. Bond cleavage frequency of PNP-IG4–PNP-IG6 by SmDexTM and its variants
469 The values on the right side indicate reaction rates. The numbers above the substrates
470 indicate bond cleavage frequencies.

471 Fig. 4. Percentage compositions of products in dextran hydrolysates
472 Glucose (*white*), IG2 (*light gray*), IG3 (*dark gray*), IG4 (*black*), and IG5 (*dot*) at 2, 8,
473 and 24 h; (A) $[\text{dextran}]_0 = 4 \text{ mg}\cdot\text{mL}^{-1}$; (B) $[\text{dextran}]_0 = 40 \text{ mg}\cdot\text{mL}^{-1}$.

A



B

279
▼

SmDex : QSWNWWSHSQVE
 Q54443 : QSWNWWSHSQVE
 Q76EQ4 : QSWNWWSHSKVE
 A4F2S5 : QDWNTWSGSEID
 Q1MVS0 : QDWNTWSGSEID
 Q8VLP4 : QDWNTWSGSEID
 P39653 : QDWNTWSGSEID
 Q59979 : QKWNTWSHTQVD
 MT-1 : Q-WS---HSQVE
 MT-2 : D-LS---HSQVE
 MT-3 : D-LF---NSQVE
 MT-4 : D-LF---NRQVE
 CITase-Bc : D-LF---NREIS
 P70873 : D-LF---NRQIS
 G9MBW2 : D-LF---NREIS
 Q8A368 : D-IA---NRPVH
 Q6VUH2 : D-IA---NRPVA
 Q6VUG9 : D-IA---NRQVS
 Q6VUG7 : D-IA---NREVS
 B0KBZ7 : D-IA---NRDIY
 Q6VUH6 : D-WS---GRMIY
 Q6VUH4 : D-WS---GRPIY
 H2EI27 : D-LL---GRTLY
 A8F6K5 : D--AWWRKRYIS

Figure 1. Klahan et al

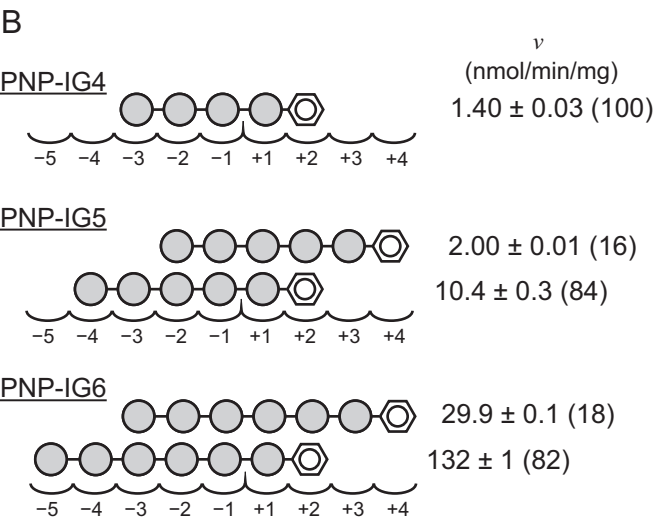
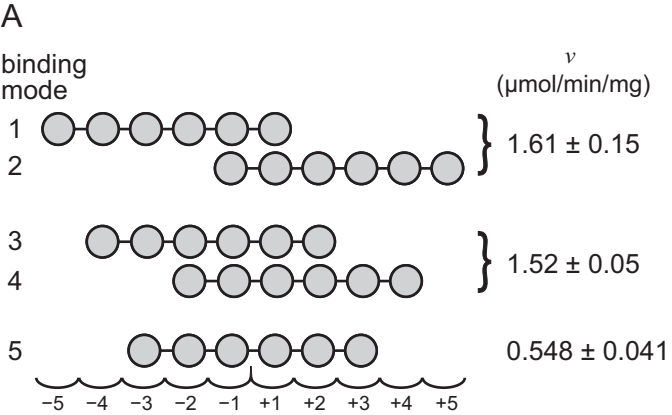
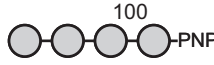
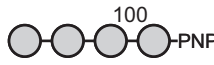
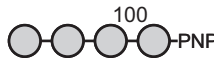
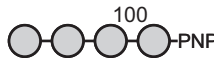
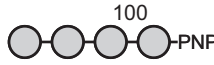
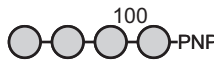
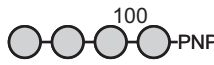


Figure 2. Klahan et al

PNP-IG4

	v (nmol/min/mg)
W279A  -PNP	0.60 ± 0.01
W279F  -PNP	1.0 ± 0.1
T558H  -PNP	2.1 ± 0.02
T563N  -PNP	2.5 ± 0.05
W279A/T563N  -PNP	0.69 ± 0.08
W279F/T563N  -PNP	0.98 ± 0.06
SmDexTM  -PNP	1.4 ± 0.0

PNP-IG5

W279A  -PNP	7.3 ± 0.1
W279F  -PNP	12 ± 1
T558H  -PNP	24 ± 1
T563N  -PNP	21 ± 1
W279A/T563N  -PNP	33 ± 1
W279F/T563N  -PNP	20 ± 1
SmDexTM  -PNP	12 ± 1

PNP-IG6

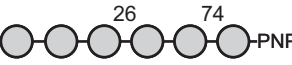
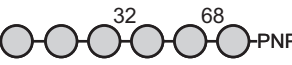
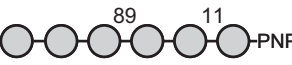
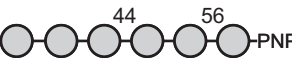
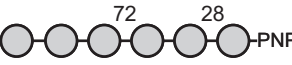
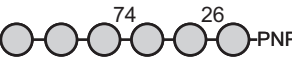
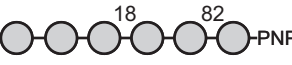
W279A  -PNP	200 ± 1
W279F  -PNP	120 ± 3
T558H  -PNP	150 ± 1
T563N  -PNP	140 ± 1
W279A/T563N  -PNP	82 ± 1
W279F/T563N  -PNP	88 ± 1
SmDexTM  -PNP	162 ± 1

Figure 3. Klahan et al

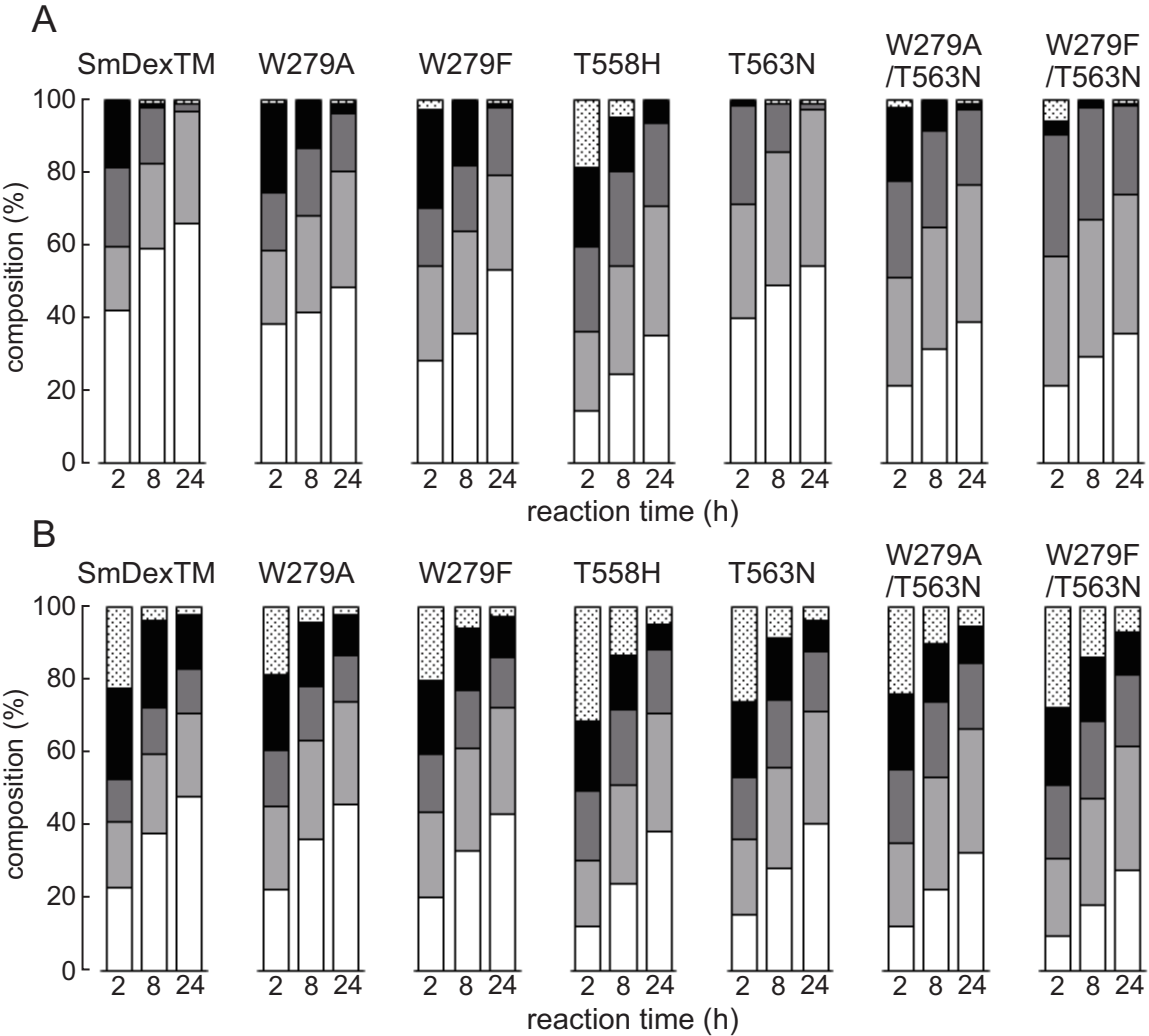


Figure 4. Klahan et al